

Article

# Observations on Nanoscale Te Precipitates in CdZnTe Crystals Grown by the Traveling Heater Method Using High Resolution Transmission Electron Microscopy

Boru Zhou <sup>1,2,\*</sup>, Wanqi Jie <sup>1,2</sup>, Tao Wang <sup>1,2</sup>, Zongde Kou <sup>1</sup>, Dou Zhao <sup>1,2</sup>, Liying Yin <sup>1,2</sup>, Fan Yang <sup>1,2</sup>, Shouzhi Xi <sup>1,2</sup>, Gangqiang Zha <sup>1,2</sup> and Ziang Yin <sup>1,2</sup>

<sup>1</sup> State Key Laboratory of Solidification Processing, Northwestern Polytechnical University, Xi'an 710072, China; jwq@nwpu.edu.cn (W.J.); taowang@nwpu.edu.cn (T.W.); kezideanm@126.com (Z.K.); z.dou@mail.nwpu.edu.cn (D.Z.); yinliying324@gmail.com (L.Y.); yang2012100392@163.com (F.Y.); xiaola507@163.com (S.X.); zha\_gq@nwpu.edu.cn (G.Z.); yindy90@mail.nwpu.edu.cn (Z.Y.)

<sup>2</sup> Key Laboratory of Radiation Detection Materials and Devices, Ministry of Industry and Information Technology, School of Materials Science and Engineering, Northwestern Polytechnical University, Xi'an 710072, China

\* Correspondence: zhoubr@mail.nwpu.edu.cn; Tel.: +86-29-8846-0445

Received: 20 December 2017; Accepted: 8 January 2018; Published: 10 January 2018

**Abstract:** Te precipitates in CdZnTe (CZT) crystals grown by the traveling heater method (THM) are investigated using high-resolution transmission electron microscopy (HRTEM). The results show that in THM-grown CZT crystals, Te precipitates are less than 10 nm in size—much smaller than those in Bridgman-grown CZT. They have hexagonal structure and form a coherent interface with zinc blend structure CZT matrix in the orientation relationship  $[\bar{1}12]_M // [0001]_P$  and  $(\bar{1}11)_M // (\bar{1}100)_P$ . A ledge growth interface with the preferred orientation along the  $[\bar{1}\bar{1}1]_M$  and  $[110]_M$  was found near Te precipitates. The growth and nucleation mechanism of Te precipitates are also discussed.

**Keywords:** transmission electron microscopy (TEM); traveling heater method; precipitation; interface structure; defects in semiconductors; CdZnTe

## 1. Introduction

Te precipitates are stubborn defects in CdZnTe (CZT) crystals which degrade the optical transmission and carrier transport properties, and restrict the application of CZT crystal for variant devices [1–3]. Te precipitates are formed by collecting super-saturated point defects such as Te anti-sites, Te interstitials, or cation vacancies, due to the retrograde solubility of Te atoms in the phase diagram. They are normally tens of nanometers in size, which is much smaller than the micrometer-scale Te inclusions formed by trapping Te-rich droplets at the growth interface during the growth process. Te inclusions have already been widely studied in the aspects of morphology evolution, formation mechanism, the effects on CZT-base device performance, etc. [1,4–7]. However, nano-scale Te precipitate seems to be more complicated and is not well understood.

The formation of Te precipitates is also thought to be related to the crystal growth method. For the popular Bridgman growth, the growth temperature is high (at the melting point of the crystal), which will produce a high density of point defects and promote the formation of Te precipitates. Rai et al. [8] characterized the density and size of Te precipitates in CZT crystals grown by Bridgman method. Te precipitates were identified to possess an average size of 20 nm and a density of  $1.3 \times 10^{16} \text{ cm}^{-3}$  in the as-grown CZT crystal. Wang et al. [9] further studied the crystal structure of Te precipitates in

CZT crystals, and three structure types (i.e., hexagonal, monoclinic, and high-pressure rhombohedral structures) were characterized.

The traveling heater method (THM) is believed to be one of most promising methods for growing high-quality CZT crystals [10] due to the lower growth temperature. Referring to the Cd-Te phase diagram and projections of  $\text{Cd}_{0.9}\text{Zn}_{0.1}\text{Te}$  solidus along the composition axis [11,12], THM growth in Te solution will decrease the growth temperature, which is favorable for lowering the solid solubility of Te atoms in as-grown CZT crystals and decreasing the possibility of Te precipitate formation.

In this work, we focus on the experimental observations of nano-scale Te precipitates in CZT crystals grown by THM using high-resolution transmission electron microscopy (HRTEM) to reveal the behaviors and underlying mechanisms of Te precipitates associated with crystal growth conditions in THM process.

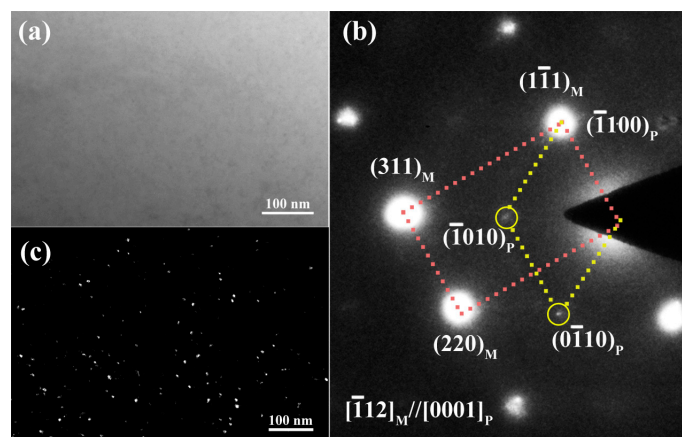
## 2. Materials and Methods

$\text{Cd}_{0.9}\text{Zn}_{0.1}\text{Te}$  crystals were grown by THM (self-designed, Xi'an, China) with the accelerated crucible rotation technique (ACRT, self-designed, Xi'an, China), as described in our previous work [13]. After the growth, the ingots were cooled to room temperature at two different cooling rates (5 °C/h and 60 °C/h). For HRTEM analyses, several single crystal specimens with the dimensions  $2.5 \times 2.5 \times 2 \text{ mm}^3$  were cut from the ingots by a diamond wire cutting machine. These specimens were mechanically ground to a thickness of 20–30  $\mu\text{m}$ , and then thinned by  $\text{Ar}^+$  ion in a plasma etching equipment (PIPC-691, Gatan, Shanghai, China) until an electron transparent thin area was acquired. A Tecnai F30 G2 transmission electron microscope (FEI, Hillsboro, OR, United States) with a spatial resolution of 0.2 nm and electron energy of 300 keV was employed to analyze the nanoscale Te precipitates and their orientation relationship with CZT matrix. For the orientation relationship analysis, electron beam diffraction method was used to confirm the results.

## 3. Results and Discussion

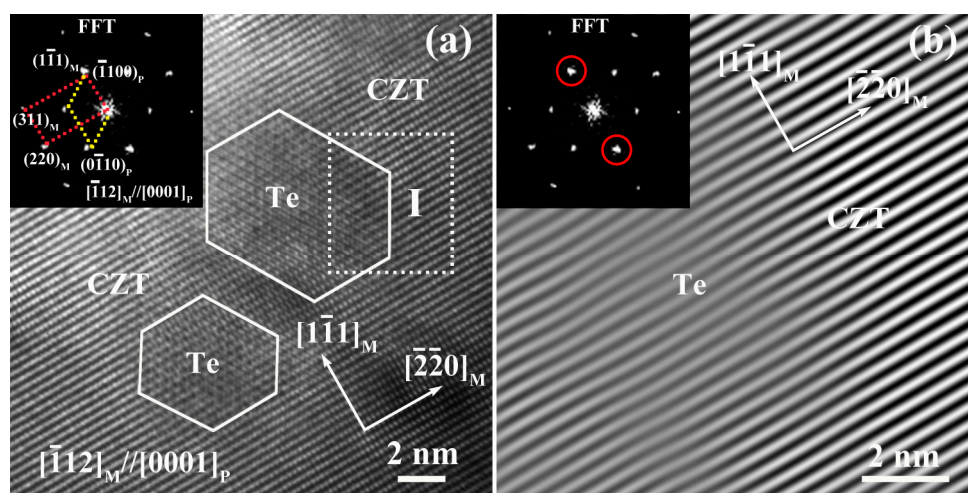
Figure 1a shows the bright-field TEM micrograph of a CZT sample. Even though Te precipitates are not visible, the selected area electron diffraction (SAED) pattern in Figure 1b shows two sets of diffraction spots. The strong diffraction spots (marked by the red rhomboid) correspond to CZT matrix phase with the zinc-blende structure (PDF number: 50–1440, space group F-43m, lattice constant 0.6456 nm) along the  $[\bar{1}12]_{\text{M}}$  zone axis. The weak spots (marked by the yellow rhomboid) are identified as Te precipitate phases with the hexagonal structure along the  $[0001]_{\text{P}}$  zone axis (PDF number: 36–1452, space group: P3121, lattice constants:  $a = 0.4458 \text{ nm}$  and  $c = 0.5927 \text{ nm}$ ). Here, the subscripts M and P represent CZT matrix and Te precipitates, respectively. The orientation relationship between Te precipitates and CZT matrix is derived to be  $[\bar{1}12]_{\text{M}} // [0001]_{\text{P}}$  and  $(1\bar{1}1)_{\text{M}} // (\bar{1}100)_{\text{P}}$ . Under hydrostatic pressure, element Te may undergo pressure-induced phase transitions from trigonal to monoclinic at about 40 kbar and from monoclinic to rhombohedral phase at about 70 kbar, respectively [14–16]. Final structures of Te precipitates are therefore decided by the internal droplet pressures. We saw only hexagonal structure in THM-grown CZT crystals, which implies that Te precipitates can be formed at a pressure less than 40 kbar or due to the confinement of CZT matrix.

Figure 1c shows the dark-field TEM micrograph corresponding to the weak diffraction spot  $(0\bar{1}10)_{\text{P}}$ . It shows that Te precipitates distribute homogeneously in CZT crystals. Different from 10–30 nm Te precipitates in Bridgman-grown CZT crystals [1,8,9], in our THM-grown CZT crystals, Te sizes were smaller than 10 nm and the density was about  $9.2 \times 10^{15} \text{ cm}^{-3}$ . The results demonstrate that THM with lower growth temperature can markedly reduce the size of Te precipitates in CZT crystals, which is favorable for improving the photoelectric properties and the structural perfection of CZT crystals.



**Figure 1.** Micrographs and selected area electron diffraction (SAED) pattern of CdZnTe (CZT) crystals grown by the traveling heater method (THM) with slow cooling rate along the  $[\bar{1}12]_M$  zone axis. (a) Bright-field transmission electron microscopy (TEM) micrograph along the  $[\bar{1}12]_M$  zone axis. (b) Dark-field TEM micrograph along the  $[\bar{1}12]_M$  zone axis. (c) SAED pattern along the  $[\bar{1}12]_M$  zone axis.

The HRTEM images of CZT sample along the  $[\bar{1}12]_M$  zone axis are shown in Figure 2. The interfaces between Te precipitates and CZT matrix were approximately outlined according to the inverse fast Fourier transform (IFFT) image. Hexagonal Te precipitates smaller than 10 nm in size were observed, shown in Figure 2a. A fast Fourier transform (FFT) pattern of region I in Figure 2a is shown in the inset of Figure 2a,b, respectively. The IFFT image was reconstructed by using the  $(\bar{1}100)_P$  spatial frequencies as marked by red circles in the FFT image, shown in Figure 2b. No lattice mismatch was found at the interface between Te precipitates and CZT matrix. This indicates a perfect coherent relationship, which may be the reason for hardly observing Te precipitates in the bright-field TEM micrograph (Figure 1a).



**Figure 2.** High-resolution TEM (HRTEM) images of Te precipitates along  $[\bar{1}12]_M$  zone axis. (a) The HRTEM image, (b) The inversed fast Fourier transform (IFFT) image of the region I in (a). The two insets are FFT patterns of region I in (a).

Figure 3a shows an HRTEM image of the specimen near the ingot tail with fast cooling rate ( $60^\circ\text{C/h}$ ) after growth, where Te precipitates in the irregular and faceted morphology were seen. A ledge growth interface was found on the edge of Te precipitates, which are parallel to the  $[1\bar{1}1]_M$

direction and perpendicular to the  $[220]_M$  direction of the CZT matrix. Therefore, the optimal growth direction of Te precipitates is along  $[\bar{1}\bar{1}1]_M$  and  $[110]_M$  in the CZT matrix, attributed to the low interfacial energies on  $\{111\}_M$  and  $\{110\}_M$  planes between CZT matrix and Te precipitate phases [17,18]. The faceted morphology of Te precipitates can be caused by a ledge growth mechanism. It is possible that the as-grown interface between Te precipitates and CZT matrix can be retained by the fast cooling rate ( $60\text{ }^\circ\text{C/h}$ ) after the growth. The irregular and faceted interface morphology (Figure 3a) indicates that the as-grown interface was obtained. Different from the coherent interface (Figure 2b) under the slowly cooling condition ( $5\text{ }^\circ\text{C/h}$ ), the dislocations labeled D and the stacking fault labeled S are seen near the as-grown interface between Te precipitates and CZT matrix along  $[110]_M$  growth direction (Figure 3b). This indicates that it is possible that the dislocations can be main channels for the diffusion and transport of Te atoms in CZT matrix, which play a crucial role in the growth process of Te precipitates in CZT matrix during cooling down.

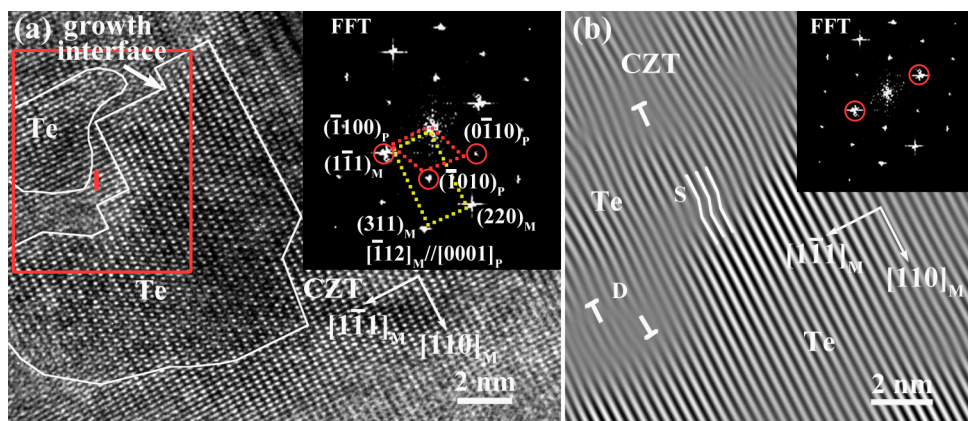


**Figure 3.** HRTEM image of the specimen near the tail of the ingot with fast cooling rate ( $60\text{ }^\circ\text{C/h}$ ) after growth. (a) The HRTEM image. (b) The inverse FFT image was reconstructed by using the  $(\bar{1}100)_P$  spatial frequencies shown in the inset of (b). The insets in (a,b) correspond to FFT patterns of region I in (a).

The formation process of Te precipitates is further illustrated in Figure 4. Te precipitates originated from the native point defect condensation [19]. Principal defects are Te interstitials, Cd vacancies, and Te anti-sites in CZT crystals when grown by THM from Te solution.  $\text{Te}_{\text{Cd}}$  anti-sites with the high migration energy barrier (1.68 eV) are almost immovable, while  $\text{Te}_i$  interstitials with a very low barrier (0.16 eV) are extremely movable along the  $[110]_M$  direction [20], which is consistent with the optimal growth direction of Te precipitates shown in Figure 3a. The migration energy barrier of  $V_{\text{Cd}}$  vacancy is 1.09 eV, between those of  $\text{Te}_{\text{Cd}}$  antisites and  $\text{Te}_i$  interstitials [20]. Therefore, Te interstitials can be the dominant diffusing species in the nucleation and growth processes of Te precipitates. After the growth, the oversaturated Te interstitial atoms aggregated to form Te precipitation nuclei due to the retrograde solidus of Te atoms in CZT matrix during the cooling of CZT crystals, as shown in Figure 4a. These nuclei caused the lattice distortions, resulting in the formation of dislocations around the nuclei. The dislocations can provide a fast channel for the diffusion and transport of Te interstitial atoms, which promote the growth of the nuclei until the whole excess Te-related point defects (priority to Te interstitials) have precipitated, as shown in Figure 4b. The real shapes of Te precipitates always mean to minimize the elastic strain energy and the total interfacial energy in order to lower the total Gibbs energy. Coherent Te precipitates have been observed in CZT matrix (Figure 2), indicating that the lattice strain energy may be very low. For nano-size Te precipitates, the interfacial energy may contribute more to the shapes of the precipitates for lowering the total system energy [21]. According to theoretical results [17],  $\{111\}$  faces have the lowest interfacial energy in zinc-blende crystal structure. Therefore, the equilibrium morphology of Te precipitates can be bounded by  $\{111\}_M$  faces and forms

a regular polygon. Therefore, the corresponding Te precipitates have also been observed, as shown in Figure 4c.

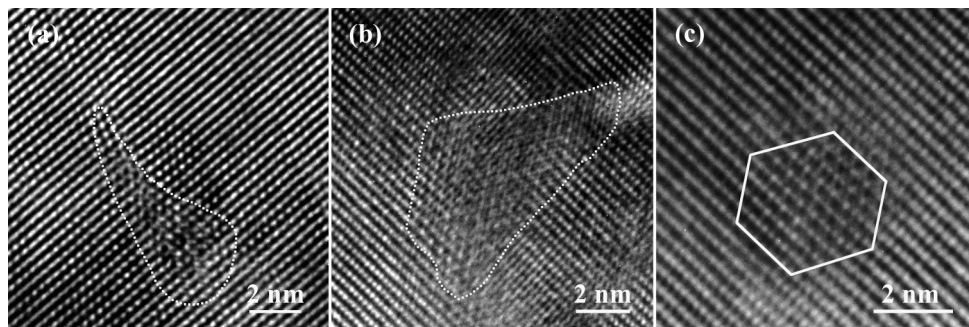


**Figure 4.** The formation process of Te precipitates: (a) nucleation; (b) growth; (c) the final morphology along the  $[\bar{1}12]_M$  zone axis.

#### 4. Conclusions

Nanoscale Te precipitates in CZT crystals grown by THM were observed using HRTEM. The majority of Te precipitates were found to be smaller than 10 nm in size with a density of  $9.2 \times 10^{15} \text{ cm}^{-3}$ —much smaller than those in Bridgman-grown CZT crystals. This demonstrates that THM with lower growth temperature is an effective way to reduce tendency to Te precipitation in CZT crystals. Moreover, Te precipitates with a hexagonal structure have a coherent interface with the CZT matrix. The orientation relationship between CZT with zinc blend structure and Te precipitates with hexagonal structure is  $[\bar{1}12]_M // [0001]_P$  and  $(1\bar{1}1)_M // (\bar{1}100)_P$ . In addition, a ledge growth interface was found on the edge of Te precipitates, and the preferred growth directions were along  $[1\bar{1}1]_M$  and  $[110]_M$  directions in the CZT matrix, attributed to their low interfacial energies.

**Acknowledgments:** This work was supported by the National Key Research and Development Program of China (2016YFB0402405, 2016YFF0101301), the National Natural Science Foundation of China (51672216, NNSFC-51502244), the Fundamental Research Funds for the Central Universities (3102016ZY011, 3102015BJ(II)ZS014), the Research Fund of the State Key Laboratory of Solidification Processing (NWPU), China (94-QZ-2014).

**Author Contributions:** Boru Zhou performed the experiments, analyzed the results and wrote the manuscript. Wanqi Jie and Tao Wang led the project, conceived the ideas, and revised the manuscript. Zongde Kou analyzed the results from the selected area electron diffraction (SAED) pattern. Dou Zhao prepared TEM specimens. Liying Yin, Fan Yang, Shouzhi Xi, Gangqiang Zha and Ziang Yin helped the manuscript and the interpretation of the results.

**Conflicts of Interest:** The authors declare no conflict of interest.

#### References

1. Rudolph, P.; Engel, A.; Schentke, I.; Grochocki, A. Distribution and genesis of inclusions in CdTe and (Cd, Zn) Te single crystals grown by the Bridgman method and by the travelling heater method. *Cryst. Growth* **1995**, *147*, 297–304. [[CrossRef](#)]
2. Carini, G.A.; Bolotnikov, A.E.; Camarda, G.S.; Wright, G.W.; James, R.B.; Li, L. Effect of Te precipitates on the performance of CdZnTe detectors. *Appl. Phys. Lett.* **2006**, *88*, 143515. [[CrossRef](#)]
3. Zhu, J.; Zhang, X.; Li, B.; Chu, J. The effects of Te precipitation on IR transmittance and crystalline quality of as-grown CdZnTe crystals. *Infrared Phys. Technol.* **1999**, *40*, 411–415. [[CrossRef](#)]
4. He, Y.; Jie, W.; Xu, Y.; Wang, T.; Zhang, G.; Yu, P.; Zheng, X.; Zhou, Y.; Liu, H. Matrix-controlled morphology evolution of Te inclusions in CdZnTe single crystal. *Scr. Mater.* **2012**, *67*, 5–8. [[CrossRef](#)]
5. Bolotnikov, A.E.; Abdul-Jabbar, N.M.; Babalola, O.S.; Camarda, G.S.; Cui, Y.; Hossain, A.M.; Jackson, E.M.; Jackson, H.C.; James, J.A.; Kohman, K.T.; et al. Effects of Te inclusions on the performance of CdZnTe radiation detectors. *IEEE Trans. Nucl. Sci.* **2008**, *55*, 2757–2764. [[CrossRef](#)]

6. Marchini, L.; Zappettini, A.; Zha, M.; Zambelli, N.; Bolotnikov, A.E.; Camarda, G.S.; James, R.B.; Marchini, L.; Zappettini, A.; Zha, M.; et al. Crystal defects in CdZnTe crystals grown by the modified low-pressure Bridgman method. *IEEE Trans. Nucl. Sci.* **2012**, *59*, 264–267. [[CrossRef](#)]
7. Roy, U.N.; Weiler, S.; Stein, J.; Hossain, A.; Camarda, G.S.; Bolotnikov, A.E.; James, R.B. Size and distribution of Te inclusions in THM as-grown CZT wafers: The effect of the rate of crystal cooling. *Cryst. Growth* **2011**, *332*, 34–38. [[CrossRef](#)]
8. Rai, R.S.; Mahajan, S.; McDevitt, S.; Johnson, C.J. Characterization of CdTe (Cd, Zn) Te, and Cd (Te, Se) single crystals by transmission electron microscopy. *Vac. Sci. Technol. B* **1991**, *235*, 1892–1896. [[CrossRef](#)]
9. Wang, T.; Jie, W.; Zeng, D. Observation of nano-scale Te precipitates in cadmium zinc telluride with HRTEM. *Mater. Sci. Eng. A* **2008**, *472*, 227–230. [[CrossRef](#)]
10. Chen, H.; Awadalla, S.A.; Iniewski, K.; Lu, P.H.; Harris, F.; Mackenzie, J.; Hasanen, T.; Chen, W.; Redden, R.; Bindley, G.J. Characterization of large cadmium zinc telluride crystals grown by traveling heater method. *J. Appl. Phys.* **2008**, *103*, 1–5. [[CrossRef](#)]
11. Haloui, A.; Feutelais, Y.; Legendre, B. Experimental study of the ternary system Cd Te Zn. *J. Alloys Compd.* **1997**, *260*, 179–192. [[CrossRef](#)]
12. Greenberga, J.H.; Guskovb, V.N. Vapor pressure scanning of non-stoichiometry in  $Cd_{0.9}Zn_{0.1}Te_{1\pm\delta}$  and  $Cd_{0.85}Zn_{0.15}Te_{1\pm\delta}$ . *J. Cryst. Growth* **2006**, *289*, 552–558.
13. Zhou, B.; Jie, W.; Wang, T.; Xu, Y.; Yang, F.; Yin, L.; Zhang, B.; Nan, R. Growth and Characterization of Detector-Grade  $Cd_{0.9}Zn_{0.1}Te$  Crystals by the Traveling Heater Method with the Accelerated Crucible Rotation Technique. *J. Electron. Mater.* **2017**, 1–6. [[CrossRef](#)]
14. Jamieson, J.C.; McWhan, D.B. Crystal structure of tellurium at high pressures. *J. Chem. Phys.* **1965**, *43*, 1149–1152. [[CrossRef](#)]
15. Aoki, K.; Shimomura, O.; Minomura, S. Crystal Structure of the High-Pressure Phase of Tellurium. *J. Phys. Soc. Jpn.* **1980**, *48*, 551–556. [[CrossRef](#)]
16. Yadava, R.D.S.; Bagai, R.B.; Borle, W.N. Theory of Te precipitation and related effects in CdTe Crystals. *J. Electron. Mater.* **1992**, *21*, 1001–1016. [[CrossRef](#)]
17. Hu, S.; Henager, C.H., Jr. Phase-field simulations of Te-precipitate morphology and evolution kinetics in Te-rich CdTe crystals. *J. Cryst. Growth*. **2009**, *311*, 3184–3194. [[CrossRef](#)]
18. Caginalp, G.; Fife, P. Higher-order phase field models and detailed anisotropy. *Phys. Rev. B* **1986**, *34*, 4940–4943. [[CrossRef](#)]
19. Rudolph, P. Fundamentals and engineering of defects. *Prog. Cryst. Growth Charact.* **2016**, *62*, 89–110. [[CrossRef](#)]
20. Lordi, V. Point defects in Cd(Zn)Te and TlBr: Theory. *J. Cryst. Growth* **2013**, *379*, 84–92. [[CrossRef](#)]
21. Solomon, E.L.S.; Araullo-Peters, V.; Allison, J.E.; Marquis, E.A. Early precipitate morphologies in Mg-Nd-(Zr). *Alloys. Scr. Mater.* **2017**, *128*, 14–17. [[CrossRef](#)]

